COMMUNICATION

Photoelectrochemical Concurrent Hydrogen Generation and Heavy Metal Recovery from Polluted Acidic Mine Water

Received 00th January 20xx,
Accepted 00th January 20xx

DOI: 10.1039/x0xx00000x

Ben Jones,[a] Katherine R. Davies,[a] Michael G. Allan,[b] S. Anantharaj,[c] Ian Mabbett, [b] Trystan Watson,[a] James R. Durrant,[a,d] Moritz F. Kuehnel,[b] Sudhagar Pitchaimuthu[a*]

The feasibility of a solar-driven photoelectrochemical process to generate hydrogen fuel from metal mine polluted water while simultaneously recovering heavy metals has been explored. Electron transport from the photoanode to the cathode plays a key role in generating hydrogen (37.6 µmol h^{-1} cm^{-2} at 0.2 V RHE, 1 sun illumination), and scavenging Zn^{2+} ions in the form of ZnO.

Hydrogen is a promising future energy carrier for carbon-free transport and electrification due to its high gravimetric energy density (142 MJ/kg), and non-polluting nature.[1] However, the current hydrogen production from methane steam reforming leaves behind a tremendous carbon footprint. In addition, fossil resources of methane are rapidly depleting, urging the development of green and sustainable alternatives to protect the environment.[2] In contrast, solar energy is clean and renewable but must be stored as chemical energy (fuel and chemicals) to meet the global energy demand at all time.[3-5] The solar hydrogen fuel generation from water using semiconductors has received profound attention since the Honda-Fujishima effect was first demonstrated in 1972.[6] The photoelectrochemical (PEC) technique shows promising performance in converting solar energy into hydrogen fuel by artificial photosynthesis.[7, 8]

The photoanode, the crucial component of a PEC cell is typically a semiconductor that generates photo charge carriers (electrons and holes) under light irradiation.[8, 9] Photoholes formed at valence band of the semiconductor oxidize water to O_2, ($2H_2O \rightarrow O_2(g) + 4H^+ + 4e^-$) and photoelectrons from the conduction band of the semiconductor anode reduce protons to H_2 at the cathode ($4H^+ + 4e^- \rightarrow 2H_2$ (g)). The overall water splitting process is an uphill reaction and thermodynamically requires 237 kJ/mol, which equals a standard potential of 1.23 V.[10] The PEC process is recognised to oxidise water at a potential more positive than +1.23 V vs NHE depending on the photoanode material, electrolyte type, and pH. In contrast, electrochemical water oxidation requires potentials >1.23 V vs. NHE for oxygen gas evolution due to high overpotential at at the anode compared to the PEC process ($2 H_2O$ (l) + Semiconductor+ $h\nu \rightarrow O_2$ (g) + 4 H^+(aq) + $4e^-$). Therefore, the number of protons derived from the anodic water oxidation process, and photoelectrons generated in the photoanode are directly dictating the hydrogen generation rate at the cathode surface. Photoelectron generation from the PEC process relies on the photoanode (light absorption), the applied potential in the circuit, charge carrier separation at electrode/electrolyte interfaces (low recombination), and resistance of the electrode and electrolyte solution. All these aspects are well-studied in PEC based solar-to-hydrogen fuel generation.[11-13] But, less attention has been paid to electrolyte engineering.

Use of fresh water has been one of the primary requirements of PEC water-splitting which when implemented in a large scale would incur additional cost for acquiring fresh water from other means such as desalination of seawater. Recent studies on life-cycle net energy assessment for PEC hydrogen generation showed that approximately 820000 m^3 of electrolyte would be required for a 1 GW facility.[14] Furthermore, adding chemicals (acid, base and salts) for enhancing the ionic conductivity of pure water (0.055 µS·cm^{-1}) in the PEC hydrogen generation process incurs additional cost[15] and creates environmental pollution issues upon discharge after the reaction. Recent demonstrations on PEC hydrogen generation using alternative electrolytes such as seawater abundantly available in oceans showed appreciable performance,[16-19] but the electrode corrosion in highly saline conditions remains a challenge. Another approach is to utilize organic water pollutants as electrolyte and feedstock in a PEC cell for offering hydrogen as a by-product.[20-23] Therefore, this method is also offering the simultaneous low-cost water treatment. However, the

[a] SPECIFIC, Materials Research Centre, Faculty of Science and Engineering, Swansea University (Bay Campus), Swansea SA18EN, United Kingdom. E-mail: S.Pitchaimuthu@swansea.ac.uk
[b] Department of Chemistry, Swansea University, Singleton Park, Swansea, SA2 8PP UK
[c] Department of Applied Chemistry, School of Advanced Science and Engineering, Waseda University, 3-4-1 Okubo, Shinjuku-ku, Tokyo 169-8555, Japan
[d] Department of Chemical Engineering, Imperial College London, Exhibition Road, London SW7 2AZ, UK
Electronic Supplementary Information (ESI) available: [QDs-sensitized TiO2 Photoanode preparation, PEC experimental condition, surface]. See DOI: 10.1039/x0xx00000x

pollutant/electrode interfaces in PEC water splitting are yet to be fully understood, and more investigations are needed.

Thousands of metal mine sites worldwide are currently not in operation that have become the major sources for heavy metals leaching and creating acid mine drainage (AMD). This metal mine pollution (so-called mine tailing) which is a potential threat to both humans and grazing animals.[24, 25] AMD pollutant sludge is already widely used in waste management (mineral industry, soil fertiliser) but its potential in water management applications is unrevealed as the heavy metals removal demands a considerable cost. The electrical conductivity of metal mine polluted water depends on heavy metal ions (Fe, Zn, Cd, Cr, Co, Ni, Cu, Pb, etc.) present in it and is typically around 1-3 mS cm^{-2}.[26] This is 10^3 times higher than that of pure water and hence, it can directly be used in PEC cell as an electrolyte without adding additional salts or chemicals. However, the acidic nature of AMD-polluted water could affect the photoanode by corrosion. It is still viable for a two-compartment PEC cell where photoanode and cathode are separated by a proton-exchange membrane (PEM). Utilizing AMD-polluted water in the cathode compartment, and alkaline or near-neutral pH electrolyte in the photoanode compartment leads to the formation of a pH gradient[27, 28] expected to form chemical bias would reduce the thermodynamic potential for water splitting[28-31]. Recent work on using AMD-contaminated water as an electrolyte in a photovoltaic panel assisted electrolysis cell showed appreciable H_2 generation at 1.48 V applied potential with stainless steel electrodes.[32] Unfortunately, uncontrollable bias from the PV panel caused a detrimental heating effect, and corrosion in the reactor and decreased the hydrogen generation efficiency. The direct solar-driven photoelectrochemical cell can avoid this issue, but to the best of our knowledge, this has not been demonstrated.

Here, we demonstrate the feasibility of using AMD-polluted water as an electrolyte in direct solar-driven PEC cells for the first time. This work explores artificial photosynthesis for H_2 generation at low overpotential with the simultaneous metal recovery. This work thus fosters PEC beyond water-splitting towards a process for water treatment and resource recovery applications.

A mesoporous TiO_2 electrode (1-micron thickness) was prepared on a fluorine-doped tin oxide (FTO)substrate and the same was coated with CdS quantum dots (QDs) using the successive ionic layer adsorption and reaction (SILAR) technique[33] (see Supporting Information). A range of different CdS QD-loaded TiO_2 photoanodes were prepared by varying the number of SILAR cycles (3, 5 and 7). These were subsequently employed in a PEC cell filled with a real AMD-contaminated water sample (cathode compartment) and a polysulfide electrolyte as a hole scavenger (photoanode compartment). The CdS quantum dot-sensitised TiO_2 electrode was used as the photoanode and kept separated from Ni mesh cathode. A $Hg/HgCl_2$ calomel electrode was used as the reference electrode with a Nafion® membrane. A detailed description of experimental conditions is given in the Supporting Information.

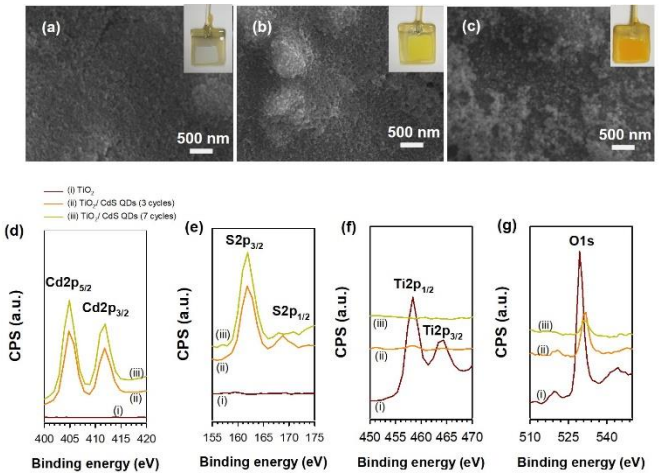

Figure 1. (a)-(c) Scanning electron images of (a) pristine TiO_2, (b) TiO_2 coated with CdS QDs (3 cycles), (c) TiO_2 coated with CdS QDs (7 cycles) (inset: respective electrode photos); (d)-(g) X-ray photoelectron spectra of pristine TiO_2, and TiO_2 coated with CdS QDs (3 &7 cycles) (d) Cd2p, (e) S2p, (f) Ti2p and (g) O1s core spectra.

Figure 1 (a)-(c) shows the surface morphology of pristine and CdS QD-coated TiO_2 photoanodes. There is a clear trend in surface topography with the number of CdS SILAR coating cycles, as displayed in **Figure 1 (b) and (c).** The nanoscale CdS particles are notable after seven cycles of SILAR as indicated by the CdS QD growth around nucleation sites. The energy-dispersive X-ray spectroscopy (EDX) analysis further ensured the CdS QD growth on the TiO_2 electrode (**Figure S1**). Consistently, the signals attributed to titanium and oxygen decrease in intensity with the increasing CdS SILAR coating cycles indicating an increase in CdS film thickness. Chemical composition of the pristine TiO_2, and CdS QD-coated TiO_2 (3 and 7 cycles) was studied using X-ray photoelectron spectroscopy (XPS). **Figure S2** shows wide scan XPS spectra. The core spectra of S 2p, Cd 2p, Ti 2p, O 1s and Zn 2p are presented in **Figure 1 (d)-(g).** The XPS peaks of Cd 3d are observed at 404.9 eV and 411.9 eV (**Figure 1 (d)**), which is in line with previous reports.[34, 35] The peaks at 161.9 eV and 163.1 eV are attributed to the characteristic of S 2p3/2 and S 2p1/2 (**Figure 1(e)**).[36] Both Cd 2d or S 1s peaks detected on TiO_2 (indexed ii and iii) that indicate CdS quantum dots formation on TiO_2 after SILAR coating. The predominant peaks at 458.5 and 464.1 eV (**Figure 1(f)**) are attributed to Ti 2p1/2 and Ti 2p3/2, respectively. A broader peak at 529.4 eV indicates O 1s, assigned to oxygen species in the TiO_2 lattice.

The Kubelka-Munk analysis (**Figure S3**) revealed the CdS QD coating on TiO_2 with a shift in the band edge from 380 to 488 nm. While increasing the CdS coating cycles from 3 to 7, the band edge gradually shifts further to 514 nm. It indicates that CdS QD growth on TiO_2 improves absorbance of visible light with the increasing coating cycle. Such an enhanced optical absorbance in the visible region of CdS QD coated TiO_2 demonstrates the suitability of the same as a photoanode in sunlight-driven catalysis. Similar SILAR coating cycles dependence optical density enhancement and absorbance edge shift at CdS QDs sensitised TiO_2 was observed by others.[37, 38] The

optimized coating cycle is 7 beyond which the properties of CdS QDs dramatically changes and appear to be that of bulk CdS with increasing thickness of CdS QDs layer. On the other hand, the high thick coating led affect the film integrity results in peel off.

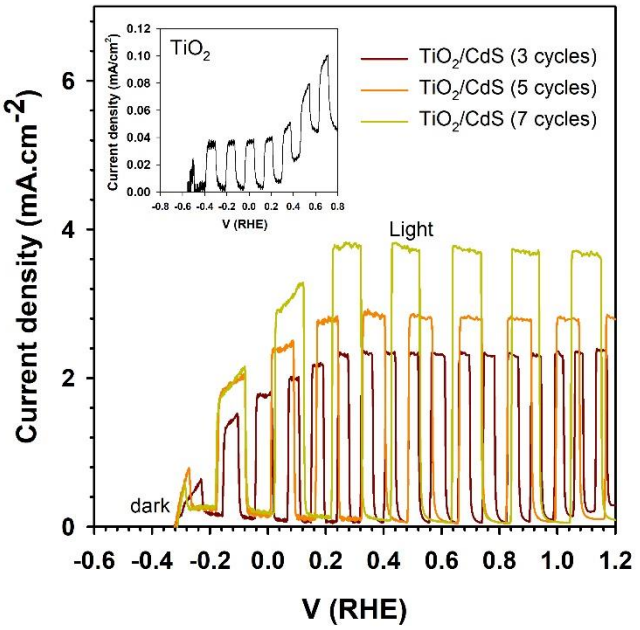

Figure 2. Chopped linear sweep voltammetry plots of TiO_2 (inset) and CdS QDs sensitised TiO_2 photoanode measured at 100 mV/s scan rate. The experiments were carried out at 1 Sun illumination conditions using a two-compartment cell. The photoanode and cathode compartments contain the 0.3 M of aqueous Na_2SO_4/Na_2S polysulfide electrolyte (pH=13). $Hg/HgCl_2$ calomel electrode used as a reference electrode in the photoanode compartment.

Before testing these photoanodes with AMD pollutants as an electrolyte, the photoelectrochemical properties of the CdS QD-sensitized TiO2 photoanode was examined in aqueous polysulfide electrolyte by chopped linear sweep voltammetry (LSV) as shown in Figure 2 which shows that photocurrent generation at the CdS QD-sensitized photoanode is gradually enhanced with the increasing CdS QD coating cycles. CdS QD coated with seven SILAR cycles exhibits a higher photocurrent density of 3.7 mA cm-2 at 0.2 V vs RHE than other photoanodes. The photoelectrochemical process at CdS QD-sensitized TiO2 can be explained explain as follows. The photoelectrons (e-) and photoholes (h+) were generated under light irradiation at the conduction band and valence band of CdS QDs, respectively. Further, the photoelectrons from the CdS conduction band were injected into the TiO_2 conduction band and then reached the charge collector (FTO substrate). Conversely, the photoholes generated at CdS valence band scavenged by the polysulfide electrolyte. The polysulfide electrolyte acts as a hole scavenger in the following manner in the photoanode compartment [39, 40].

$$SO_3^{2-} + H_2O + 2h^+_{VB^+} + 2OH^- \rightarrow SO_4^{2-} + 2H^+ + H_2O \quad (1)$$

$$2SO_3^{2-} \rightarrow S_2O_6^{2-} \quad (2)$$

$$2S^{2-} + 2h^+_{VB^+} \rightarrow S_2^{2-} \quad (3)$$

The protons (H^+) produced from equation (1) diffuse through the PEM to the cathode compartment while the photoelectrons from the photoanode are transferred via the external circuit to the Ni mesh cathode that reduces protons to H_2 as shown below in equation (4).

$$2H^+ + 2e^- \rightarrow H_2 \quad (4)$$

The hydrogen gas generated from a seven cycle CdS QD-sensitized TiO_2 photoanode was quantified to be 27 µmol h^{-1} cm^{-2} at +0.2 V vs RHE applied potential (**Figure S4**). Importantly, these CdS QD-sensitized photoanodes result in approximately 2.5 $mA.cm^{-2}$ at 0 V vs RHE, inferring H_2 generation at a much lesser applied potential in the external circuit. Different research groups have studied bias-free photoelectrochemical hydrogen generation in CdS QD-sensitized TiO_2 photoanodes,[41-43] suggesting that this PEC cell is suitable to validate photoelectron-driven catalysis reactions in AMD pollutant electrolyte too.

AMD water pollutant samples were collected from abandoned metal mine sites located in Wales (UK) and tested as an electrolyte in a two-compartment photoelectrochemical cell, and the most suitable feedstock was found to have a pH of 4.8 and contain 47.1 ppm (0.72 mmol) of Zn^{2+} ions (Supporting Information). In the photoanode compartment, aqueous 0.3 M polysulfide solution was used as an electrolyte, and AMD polluted water was placed in the cathode chamber. The chronoamperometry plots (**Figure 3a**) for different CdS QD-sensitized TiO_2 photoanodes were recorded using a three-electrode configuration as discussed above. **Figure 3a** shows that CdS QD-sensitised photoanodes results in superior PEC performance than bare TiO_2 photoanode (inset of **Figure 3a**). Among the different CdS QD-coated photoanodes, those having been coated with seven SILAR cycles showed the highest photoelectrochemical activity with an average photocurrent density of 5.5 mA cm^{-2}. Plausible reasons for the high PEC performance with this electrode are (a) enhanced light absorption and (b) sufficient coverage of CdS QDs on TiO_2 reduces charge recombination loss. The small amount of photocurrent reduction observed in all photoanodes after an hour is likely due to polysulfide scavenger degradation in the photoanode compartment. In the cathode compartment, the observed strong bubble formation indicates hydrogen gas generation (equation 4) from AMD electrolyte (**See supporting video**).

The corresponding hydrogen gas generation from these experiments was quantified through gas chromatography (**Figure 3 (b)**). Hydrogen generation showed a linear tendency against time, and the H_2 generation rate was found to increase with increasing CdS coating cycles, thus proving the role of photoelectron generation at CdS QDs for hydrogen evolution (equation 4) at the cathode. Seven SILAR cycles of CdS QDs

deposition onto TiO_2 results in a high hydrogen evolution rate of 38 µmol h^{-1} cm^{-2} at 0.2 V vs RHE applied potential. The AMD-based electrolyte yields slightly higher hydrogen gas evolution than polysulfide electrolyte (27 µ.mol/hr.cm^2) under identical experimental condition.

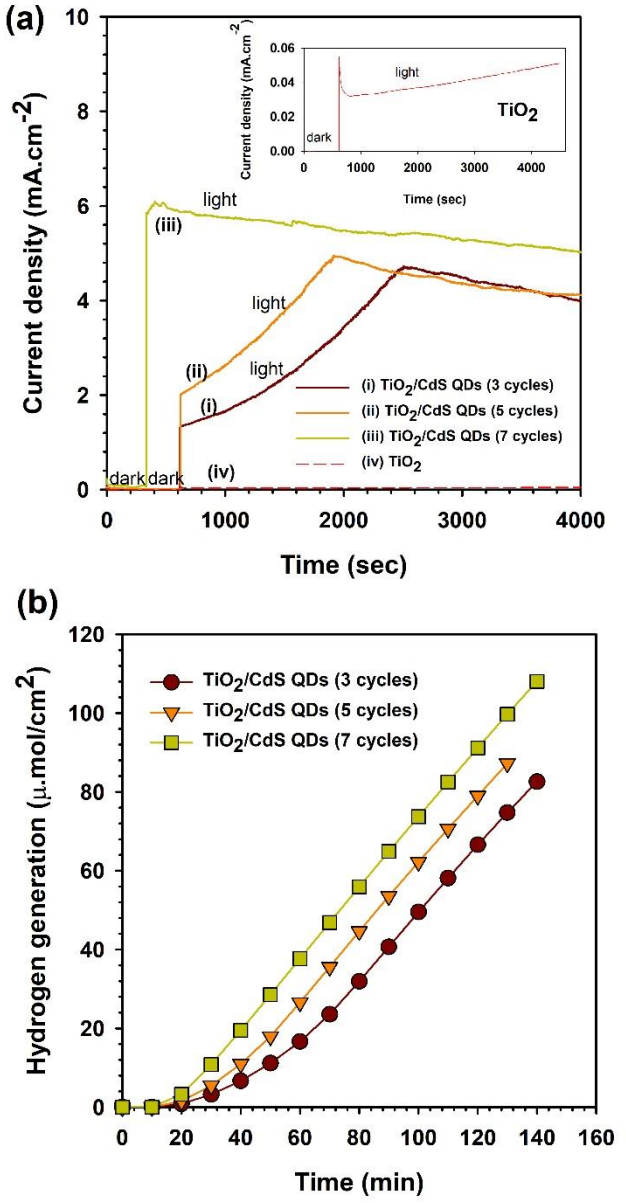

Figure 3. (a) Chronoamperometry plots of TiO_2 photoanode (inset) and TiO_2 sensitised with different CdS QDs coating cycles (3,5 and 7); (b) Quantification of H_2 evolved during PEC reactions. Both Figure 4 (a) and (b) experiments measured at 1 Sun illumination conditions. Note that 0.3 M of aqueous Na_2SO_4/Na_2S polysulfide electrolyte (pH=13) and real-time AMD pollutant (pH=4.8) are used as an electrolyte in the photoanode and cathode compartments, respectively. The measurements were recorded at 0.2 V vs RHE using $Hg/HgCl_2$ calomel reference electrode.

It infers that AMD-polluted water can be utilised as an electrolyte feedstock for solar hydrogen fuel generation. A similar PEC experiment was repeated at 2 Sunlight intensity to ensure the potency of photoelectron generation at the photoanode on hydrogen fuel generation. For instance, increasing light intensity is expected to illuminate the entire bandgap energy of CdS QDs could result in higher hydrogen gas evolution at the cathode (equation 4). After 2 h irradiation, as much as 106 µmol/cm^2 was formed under 2 Sun intensity irradiation (**Figure S5**). It is significantly higher than at 1 Sun intensity (83 µmol/cm^2) after an identical period of 2 h. We can conclude that the number of CdS QD coating cycles and the light intensity influences the PEC hydrogen generation by accelerating the photo charge carrier generation at the photoanode.

The CdS QDs has been demonstrated widely on powder-type photocatalysis compared to wired PEC configuration for solar hydrogen generation. Mostly aqueous polysulfide (S_x^-/S^-) is used for electrolyte.[44] Typically, powder-type CdS QDs are exhibiting in the order of 0.5-10 m.mol/g/hr hydrogen gas generation, and wired PEC configuration results in the order of 10 µmol to 1 m.mol/cm^2/hr. The CdS QDs based photocatalysis and PEC based solar fuel generation depend on metal oxide support (TiO_2, ZnO, SnO_2)[45, 46], co-catalyst (MoS_2, Ag)[47, 48,49] and co-sensitizer coatings (CdSe, PbS, InP)[50, 51]. The present work on CdS QDs coated TiO_2 photoanode generates 83 µmol/cm^2 hydrogen generation from metal mine polluted water is comparable with polysulfide electrolyte.

One can raise the question about heavy metals (Zn) present in the AMD-polluted water during the PEC reaction. It has been widely reported that photoelectrons generated from the photocatalyst surface could reduce the heavy metals (Cr, Pb, Cd, etc.) in the electrolyte.[52-55] Mostly, this reaction occurs through chemisorption, reduction, and desorption processes of heavy metal ions on the electrode surface. But Zn^{2+} is one of a few metal ions that cannot be reduced to its metallic state in an electrolyte of pH 4.8 even though we examined the surface of Ni mesh cathode before and after the PEC reaction.

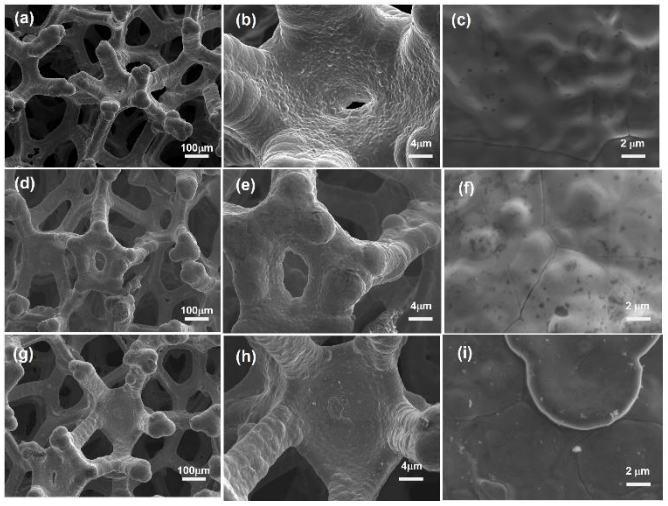

Figure 4. (a)- (c) FESEM images of Ni mesh before involved in PEC reaction, measured at different magnification scales (100 µm, 4 µm and 2 µm); (d)-(e) FESEM images of Ni mesh after involved in PEC reaction, measured at different magnification scales (100 µm, 4 µm and 2 µm) (the photoanode- 3 cycles of CdS QDs coated TiO_2); (g)-(i) FESEM images of Ni

mesh after involved in PEC reaction measured at different magnification scales (100 µm, 4 µm and 2 µm) (the photoanode- 7 cycles of CdS QD coated TiO_2).

The SEM images of the Ni cathode before and after PEC reaction are summarised in **Figure 4 (a-i)**. It is challenging to recognise surface modifications from the low magnification SEM images (100 and 4 µm scale). High magnification SEM images at 2 µm scale (**Figure 4 (c), (f)** and **(i)**) reveal surface changes occurred on Ni mesh after PEC reaction. Further analysing the SEM images at 1 µm scale (**Figure S6 (b)**), a fish scale-type layer deposition was noticed on the Ni cathode after a PEC experiment with a 7 CdS QDs cycles photoanode. Formation of the fish scale-type layer might be due to electrochemical deposition of Zn^{2+} metal ions present in the AMD electrolyte to ZnO. A similar approach on arsenic heavy metals leaching from anode material was recovered at cathode surface by electrochemical technique.[56]

Here, photoelectrons generated from the photoanode are transported to the cathode and drive this reaction. The fish scales-type layer is discernible only at the Ni cathode coupled to the 7-cycles photoanode, not at the 3-cycle photoanode, implying that the Ni cathode surface modification varies with photoelectron collection from the photoanode. When the HER is vigorous at the cathode due to such an increased photocurrent, the local pH is expected to sufficiently increase due to H^+ consumption that is just enough to precipitate Zn^{2+} as $Zn(OH)_2$.

Further examining the surface of these Ni mesh cathodes shed more light on this issue. The wide scan XPS spectra and Zn2p, O1S core spectra of the Ni mesh cathode recorded before and after PEC reaction clearly explain the origin of surface modification at Ni cathode. The wide scan XPS (**Figure S7**) showed an additional Zn peak with the native Ni peak of the cathode, and these Zn peaks might be attributed to ZnO formation by Zn^{2+} cations deposition at Ni cathode due to the sufficiently high localized alkalinity due to vigorous H_2 evolution. Further analysing Zn 2p core spectra (**Figure 5a**), a distinguished shoulder peak of Zn $2p_{3/2}$ at 1020.5 eV confirms ZnO formation[57, 58]. Further analysing O 1s peaks (**Figure 5b**) of the reference Ni mesh sample showed peaks at 532.1, and 533.4 eV, indicating the presence of ZnO and Ni $(OH)_x$, respectively. In Ni mesh after PEC reactions, Zn^{2+} ions deposition results in ZnO as it is catalysed on $Ni(OH)_x$ surface instead of metallic Ni surface (marked as "ii" and "iii" in Figure 5b) as $Ni(OH)_x$ is inherently present in the commercial Ni mesh product. This is why the ZnO layer is evidenced at Ni mesh used in 7 CdS cycles photoanode assisted PEC reaction. Similar multistep reactions were previously reported on the anodic or cathodic electrochemical deposition of ZnO in an acidic environment under the applied potential (-0.8 to-1.3 V).[59, 60] A distinct shift noticed in the O 1s peak from 532.1 to lower binding energy of 530.5 eV confirms the ZnO formation on the Ni mesh (**Figure 5b)**. Therefore, the XPS results strongly suggest that OH groups present on the Ni mesh and the localized alkalinity created due to vigorous hydrogen evolution mediate Zn heavy metals recovery in the form of ZnO.

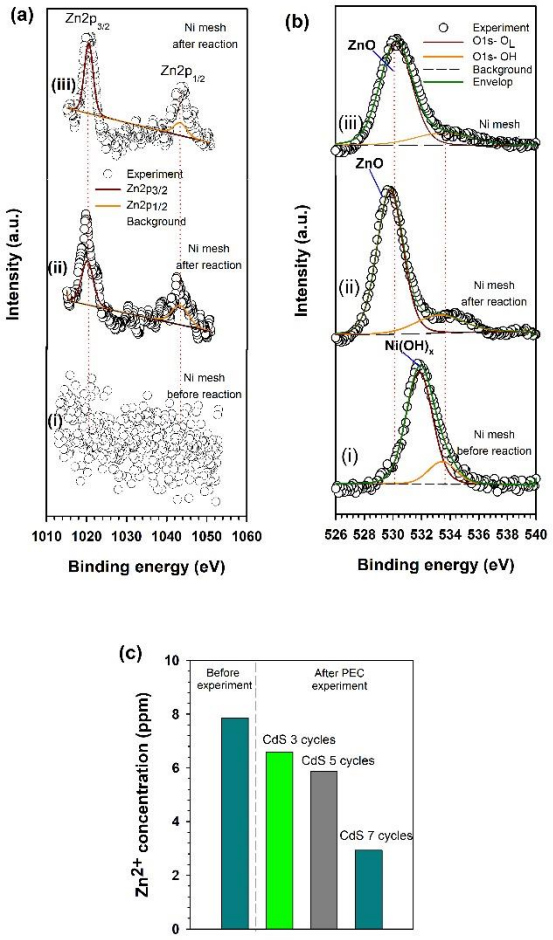

Figure 5. The XPS core spectra results of (a) Zn 2p and (b) O1s core spectra recorded from Ni mesh before and after PEC experiments. Note that the Ni mesh cathode was kept in the cathode compartment of PEC cells. The reference Ni mesh sample before the PEC process is marked as "i". The Ni mesh after PEC experiments - with 3 CdS QD cycles coated TiO_2 marked as "ii", and 7 CdS QD cycles coated TiO_2 mentioned as "iii". OL- lattice oxygen, OH- hydroxyl group. The Zn^{2+} ions concentration (ppm) before after PEC treatment using different photoanodes.

In order to verify the Zn^{2+} ions removal from the electrolyte the Zn concentration has measured before and after PEC experiments were using plasma couple atomic absorption spectroscopy (**Figure 5c**). It is found that the Zn concentration has reduced from 7.85 ppm to 2.96 ppm after PEC treatment. The high removal rate at 7 cycle coated CdS QDs TiO_2 photoanode might due to higher amount of photoelectrons generation which facilitate the electrochemical reaction at cathode.

Based on the above results, we propose a possible photoelectrochemical hydrogen generation mechanism and metal recovery from AMD polluted water, as illustrated in **Figure 6**. The CdS QDs-sensitized TiO_2 photoanode generates

photo charge carriers (electrons and holes) under simulated solar light illumination. The photo holes scavenged by polysulfide ions undergo redox reactions and produce protons (H^+). Meanwhile, photoelectrons transported to the cathode reduce the protons/water molecules to hydrogen gas. Concurrently, a heavy metal (Zn^{2+}) present in the AMD is deposited on the cathode catalysed by surface OH and localized alkalinity created by vigorous hydrogen evolution are recovered in the form of ZnO after the reaction. The current work majorly focuses on hydrogen fuel generation, but further experiments of quantifying Zn^{2+} metal ions in the cathode compartment, before and after PEC reaction, will explain the heavy metal recovery pathways. We have tested different cathodes such as Pt, stainless steel, and Ti, in addition to Ni mesh. In comparison, the Ni mesh showed the highest stability. Still, high surface area-based two-dimensional materials (graphene composite, MoS_2, MXenes, etc.), chalcogenide semiconductors, or carbon-based cathodes that may be used in these experiments are expected to reduce the cost.

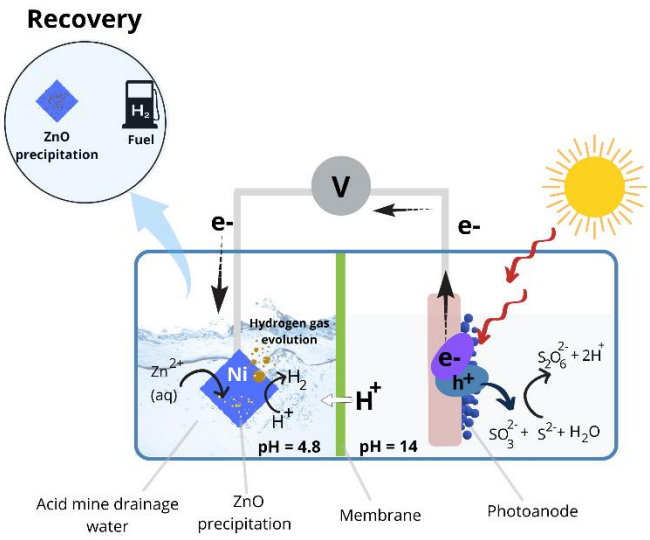

Figure 6. Schematic illustration of AMD polluted water feedstock-based PEC cells, and proposed mechanism for hydrogen generation, and heavy metals recovery. Real AMD water samples collected from an abandoned metal mine site at Frongoch, Mid Wales region in the UK was used as an electrolyte in the cathode compartment (AMD samples kindly supplied by Natural Resources Wales, Cardiff, UK).

Overall, the proton reduction to hydrogen gas showed high priority compared to metal recovery reaction. According to Brooks et al.,[11] the photoelectron-driven reduction of Zn^{2+} cation is slower than hydrogen generation when the electrolyte is diluted with a high amount of water. It infers that the absence of electron scavengers or metal-binding agents in the aqueous electrolyte results in the weak metal reduction reaction. Therefore, modifying the AMD polluted electrolyte with an appropriate organic solvent may result in high metal recovery rather than hydrogen gas evolution. However, recovery of Zn as ZnO even in smaller quantity is complementary to solar hydrogen fuel generation. This present work is first-of-its-kind in PEC process-based simultaneous hydrogen generation with a heavy metal recovery from real-world AMD water.

Conclusions

We demonstrated real-world acid mine drainage (AMD) polluted water collected from abandoned metal mine site as a potential electrolyte in solar hydrogen fuel generation, and heavy metals recovery using a CdS QD-sensitized TiO_2 photoanode and a Ni mesh cathode. Photoelectrons generated at CdS QD-sensitized TiO_2 photoanode modulated by varying the number of QD coating cycles and the light intensity. We observed as high as ~85 and 106 µmol/cm^2 of hydrogen gas evolution at 2 h reaction under 1 and 2 sun illumination, respectively. Single metal (Zn) AMD polluted water was tested in the current work. Multi metal-based real-world AMD pollutants are to be tried for validating their potential in PEC reactions. Polysulfide sacrificial electrolyte in the photoanode compartment can be replaced with non-corrosive organic water pollutants, or biomass substances to oxidise and convert them into toxic-free mineral by-products. A simultaneous water pollutant treatment at a photoanode and solar fuel generation at the cathode along with a heavy metal recovery open new pathways beyond the water-splitting process. Further understanding of AMD pollutants/electrode interfaces through in-operando tools are appreciable compared to conventional post-processing analysis.

Acknowledgements

This work is part-funded by the European Social Fund (ESF) through the European Union's Convergence programme administered by the Welsh Government (KESS-II program) and Ser Cymru-II Rising Star Fellowship (80761-SU-102 (West)). We thank Natural Resources Wales (NRW) for partial financial support to demonstrate this project through KESS-II program at Swansea University. SP sincerely thank Peter Stanley for providing the AMD water samples from different Mid Wales regions, UK. M.F.K. acknowledges startup funding from Swansea University. M.G.A. thanks EPSRC for a DTP studentship (EP/R51312x/1).

Author Contributions

SP conceived the concept, designed the research work, and wrote the manuscript with all the authors' input and comments. The photoanode sample preparation and photoelectrochemical experiments were performed by BJ with assistance by KD. MGA carried out the hydrogen gas evolution experiment. SA interpreted the deposition of ZnO and correlated with other experimental studies and also involved in manuscript preparation. MFK contributed technical input, manuscript preparation, designed the hydrogen gas measurement setup and supervised the hydrogen

evolution studies. JRD act as advisor of the project and provided technical inputs. IM and TW facilitated necessary support for XPS and optical measurements.

Conflicts of interest

There are no conflicts to declare.

Notes and references

1. A. Züttel, A. Remhof, A. Borgschulte and O. Friedrichs, *Philosophical Transactions of the Royal Society A: Mathematical, Physical and Engineering Sciences*, 2010, **368**, 3329-3342.
2. J. A. Turner, *Science*, 2004, **305**, 972-974.
3. N. S. Lewis and D. G. Nocera, *Proceedings of the National Academy of Sciences*, 2006, **103**, 15729-15735.
4. Y. Tachibana, L. Vayssieres and J. R. Durrant, *Nature Photonics*, 2012, **6**, 511-518.
5. N. S. Lewis, *Science*, 2016, **351**, aad1920.
6. A. Fujishima and K. Honda, *Nature*, 1972, **238**, 37-38.
7. A. Harriman, *Nature*, 1978, **276**, 15-16.
8. G. Hodes, J. Manassen and D. Cahen, *Nature*, 1976, **261**, 403-404.
9. G. Hodes, *The Journal of Physical Chemistry Letters*, 2012, **3**, 1208-1213.
10. M. G. Walter, E. L. Warren, J. R. McKone, S. W. Boettcher, Q. Mi, E. A. Santori and N. S. Lewis, *Chemical Reviews*, 2010, **110**, 6446-6473.
11. A. C. Brooks, K. Basore and S. Bernhard, *Inorganic Chemistry*, 2013, **52**, 5794-5800.
12. J. H. Kim, D. Hansora, P. Sharma, J.-W. Jang and J. S. Lee, *Chemical Society Reviews*, 2019, **48**, 1908-1971.
13. C. Ros, T. Andreu and J. R. Morante, *Journal of Materials Chemistry A*, 2020, **8**, 10625-10669.
14. R. Sathre, C. D. Scown, W. R. Morrow, J. C. Stevens, I. D. Sharp, J. W. Ager, K. Walczak, F. A. Houle and J. B. Greenblatt, *Energy & Environmental Science*, 2014, **7**, 3264-3278.
15. S. Crawford, E. Thimsen and P. Biswas, *Journal of The Electrochemical Society*, 2009, **156**, H346.
16. S. Ichikawa, *International Journal of Hydrogen Energy*, 1997, **22**, 675-678.
17. Y. Li, J. Feng, H. Li, X. Wei, R. Wang and A. Zhou, *International Journal of Hydrogen Energy*, 2016, **41**, 4096-4105.
18. M. Jadwiszczak, K. Jakubow-Piotrowska, P. Kedzierzawski, K. Bienkowski and J. Augustynski, *Advanced Energy Materials*, 2020, **10**, 1903213.
19. M. M. Ayyub, M. Chhetri, U. Gupta, A. Roy and C. N. R. Rao, *Chemistry – A European Journal*, 2018, **24**, 18455-18462.
20. M. S. Koo, K. Cho, J. Yoon and W. Choi, *Environmental Science & Technology*, 2017, **51**, 6590-6598.
21. D. Pan, S. Xiao, X. Chen, R. Li, Y. Cao, D. Zhang, S. Pu, Z. Li, G. Li and H. Li, *Environmental Science & Technology*, 2019, **53**, 3697-3706.
22. L. Sun, Y. Wang, F. Raziq, Y. Qu, L. Bai and L. Jing, *Scientific Reports*, 2017, **7**, 1303.
23. C. Wu, Z. Gao, S. Gao, Q. Wang, H. Xu, Z. Wang, B. Huang and Y. Dai, *Journal of Energy Chemistry*, 2016, **25**, 726-733.
24. A. RoyChowdhury, D. Sarkar and R. Datta, *Current Pollution Reports*, 2015, **1**, 131-141.
25. W. Salomons, *Journal of Geochemical Exploration*, 1995, **52**, 5-23.
26. C. N. Kien, N. V. Noi, L. T. Son, H. M. Ngoc, S. Tanaka, T. Nishina and K. Iwasaki, *Soil Science and Plant Nutrition*, 2010, **56**, 344-356.
27. D. A. Vermaas, S. Wiegman, T. Nagaki and W. A. Smith, *Sustainable Energy & Fuels*, 2018, **2**, 2006-2015.
28. K. Sun, R. Liu, Y. Chen, E. Verlage, N. S. Lewis and C. Xiang, *Advanced Energy Materials*, 2016, **6**, 1600379.
29. S. Anantharaj, K. Karthik, T. S. Amarnath, S. Chatterjee, E. Subhashini, K. C. Swaathini, P. E. Karthick and S. Kundu, *Applied Surface Science*, 2019, **478**, 784-792.
30. L. Chen, X. Dong, F. Wang, Y. Wang and Y. Xia, *Chemical Communications*, 2016, **52**, 3147-3150.
31. W. Zhu, W. Zhang, Y. Li, Z. Yue, M. Ren, Y. Zhang, N. M. Saleh and J. Wang, *Journal of Materials Chemistry A*, 2018, **6**, 24277-24284.
32. F. Castelan Marques, G. Mendonça Valane and V. Mezadre Buzato, *International Journal of Energy Research*, 2020, **44**, 12188-12196.
33. P. Sudhagar, J. H. Jung, S. Park, R. Sathyamoorthy, H. Ahn and Y. S. Kang, *Electrochimica Acta*, 2009, **55**, 113-117.
34. A. Subramanian, D. Punnoose, S. S. Rao, C. Venkata Thulasi Varma, B. Naresh, V. Raman and H.-J. Kim, *New Journal of Chemistry*, 2017, **41**, 5942-5949.
35. Y. Liu, F. Dai, R. Zhao, X. Huai, J. Han and L. Wang, *Journal of Materials Science*, 2019, **54**, 8571-8580.
36. M. J. Jackman, A. G. Thomas and C. Muryn, *The Journal of Physical Chemistry C*, 2015, **119**, 13682-13690.
37. A. G. Aragon, W. Kierulf-Vieira, T. Łęcki, K. Zarębska, J. Widera-Kalinowska and M. Skompska, *Electrochimica Acta*, 2019, **314**, 73-80.
38. E. Rabinovich and G. Hodes, *The Journal of Physical Chemistry C*, 2013, **117**, 1611-1620.
39. V. N. Rao, S. Pitchaimuthu, P. Ravi, M. Sathish, H. Han and S. M. Venkatakrishnan, *ChemCatChem*, 2020, **12**, 3139-3152.
40. N. Buehler, K. Meier and J. F. Reber, *The Journal of Physical Chemistry*, 1984, **88**, 3261-3268.
41. R. Raja, P. Sudhagar, A. Devadoss, C. Terashima, L. K. Shrestha, K. Nakata, R. Jayavel, K. Ariga and A. Fujishima, *Chemical Communications*, 2015, **51**, 522-525.
42. P. Rodenas, T. Song, P. Sudhagar, G. Marzari, H. Han, L. Badia-Bou, S. Gimenez, F. Fabregat-Santiago, I. Mora-Sero, J. Bisquert, U. Paik and Y. S. Kang, *Advanced Energy Materials*, 2013, **3**, 176-182.
43. R. Trevisan, P. Rodenas, V. Gonzalez-Pedro, C. Sima, R. S. Sanchez, E. M. Barea, I. Mora-Sero, F. Fabregat-Santiago and S. Gimenez, *The Journal of Physical Chemistry Letters*, 2013, **4**, 141-146.
44. L. Jin, H. Zhao, Z. M. Wang and F. Rosei, *Advanced Energy Materials*, 2021, **11**, 2003233.
45. P. S. Shinde, J. W. Park, M. A. Mahadik, J. Ryu, J. H. Park, Y.-J. Yi and J. S. Jang, *International Journal of Hydrogen Energy*, 2016, **41**, 21078-21087.
46. W. Wang, C. Jin and L. Qi, *Small*, 2018, **14**, 1801352.
47. B. Han and Y. H. Hu, *Energy Science & Engineering*, 2016, **4**, 285-304.

48. Y. Zhang, C. Yuan, Q. Wang, M. R. Hoffmann, X. Zhang, J. Nie, C. Hu, S. Chen, J. Qiao, Q. Wang and Y. Cong, *Electrochimica Acta*, 2019, **328**, 135124.
49. S. R. Kadam, S. W. Gosavi, B. B. Kale, N. Suzuki, C. Terashima and A. Fujishima, *Journal*, 2019, **9**, 12036.
50. Z.-J. Li, X.-B. Fan, X.-B. Li, J.-X. Li, F. Zhan, Y. Tao, X. Zhang, Q.-Y. Kong, N.-J. Zhao, J.-P. Zhang, C. Ye, Y.-J. Gao, X.-Z. Wang, Q.-Y. Meng, K. Feng, B. Chen, C.-H. Tung and L.-Z. Wu, *Journal of Materials Chemistry A*, 2017, **5**, 10365-10373.
51. D. W. Su, J. Ran, Z. W. Zhuang, C. Chen, S. Z. Qiao, Y. D. Li and G. X. Wang, *Science Advances*, 2020, **6**, eaaz8447.
52. D. Chen and A. K. Ray, *Chemical Engineering Science*, 2001, **56**, 1561-1570.
53. C. Singh and R. Chaudhary, *Journal of Renewable and Sustainable Energy*, 2013, **5**, 053102.
54. L. X. Chen, T. Rajh, O. Mićic, Z. Wang, D. M. Tiede and M. Thurnauer, *Nuclear Instruments and Methods in Physics Research Section B: Beam Interactions with Materials and Atoms*, 1997, **133**, 8-14.
55. F. Hosseini and S. Mohebbi, *Journal of Industrial and Engineering Chemistry*, 2020, **85**, 190-195.
56. R. Beltrán-Suito, V. Forstner, J. N. Hausmann, S. Mebs, J. Schmidt, I. Zaharieva, K. Laun, I. Zebger, H. Dau, P. W. Menezes and M. Driess, *Chemical Science*, 2020, **11**, 11834-11842.
57. L. S. Dake, D. R. Baer and J. M. Zachara, *Surface and Interface Analysis*, 1989, **14**, 71-75.
58. C. D. Wagner and G. E. Muilenberg, *Handbook of x-ray photoelectron spectroscopy : a reference book of standard data for use in x-ray photoelectron spectroscopy*, Physical Electronics Division, Perkin-Elmer Corp., Eden Prairie, Minn., 1979.
59. J. S. Wellings, N. B. Chaure, S. N. Heavens and I. M. Dharmadasa, *Thin Solid Films*, 2008, **516**, 3893-3898.
60. M. Skompska and K. Zarębska, *Electrochimica Acta*, 2014, **127**, 467-488.

